

Syntheses, structures and magnetic properties of azido- and phenoxo-bridged complexes of manganese containing tridentate aroylhydrazone based ligands



Hassan Hosseini-Monfared^{a,*}, Rahman Bikas^a, Joaquín Sanchiz^{b,*}, Tadeusz Lis^c, Milosz Siczek^c, Jiri Tucek^c, Radek Zboril^d, Peter Mayer^e

^a Department of Chemistry, University of Zanjan, 45195-313 Zanjan, Iran

^b Departamento de Química Inorgánica, Universidad de La Laguna, 38206 La Laguna, Tenerife, Spain

^c Faculty of Chemistry, University of Wrocław, Joliot-Curie 14, Wrocław 50-383, Poland

^d Regional Centre of Advanced Technologies and Materials, Faculty of Science, Department of Physical Chemistry, Faculty of Science, Palacky University, 17. listopadu 1192/12, in Olomouc, 771 46 Olomouc, Czech Republic

^e Fakultät für Chemie und Pharmazie, Ludwig-Maximilians-Universität, München, Butenandtstr. 5-13, Haus D, D-81377 München, Germany

ARTICLE INFO

Article history:

Received 14 March 2013

Accepted 19 May 2013

Available online 27 May 2013

Keywords:

Dinuclear Mn complexes

Magnetic behavior

Azide

Coordination polymer

Hydrazones

ABSTRACT

Five new compounds have been prepared by the reaction of $\text{MnCl}_2 \cdot 4\text{H}_2\text{O}$ with aroylhydrazone in the presence of NaN_3 : $[\text{Mn}(\text{L}^1)(\text{N}_3)(\text{HOCH}_3)_2]_2$ (**1**), $[\text{Mn}(\text{L}^2)(\text{N}_3)(\text{HOCH}_3)_2]_2$ (**2**), $[\text{Mn}(\text{L}^3)(\text{N}_3)(\text{HOCH}_3)_{0.75}(\text{EtOH})_{0.25}]_2$ (**3**), $[\text{Mn}(\text{L}^4)(\text{N}_3)(\text{HOCH}_3)_2]_2$ (**4**) and $[\text{Mn}_2(\text{L}^5)_2(\text{HOCH}_3)_2]_n$ (**5**). ($\text{HL}^1 = (E)$ -3-hydroxy- N' -(1-(pyridin-2-yl)ethylidene)-2-naphthohydrazide, $\text{HL}^2 = (E)$ - N' -(phenyl(pyridin-2-yl)methylene)furan-2-carbohydrazide, $\text{H}_2\text{L}^3 = (Z)$ - N' -(4-oxo-4-phenylbut-2-en-2-yl)isonicotinohydrazide, $\text{H}_2\text{L}^4 = (E)$ - N' -(5-bromo-2-hydroxybenzylidene)isonicotinohydrazide). In absence of NaN_3 the mononuclear complex $[\text{Mn}(\text{H}_2\text{L}^5)_2(\text{EtOH})_2\text{Cl}_2]$ (**6**) was obtained by the reaction of $\text{MnCl}_2 \cdot 4\text{H}_2\text{O}$ and H_2L^5 ((E) - N' -(2-hydroxy-3-methoxybenzylidene)isonicotinohydrazide). All the compounds have been characterized by elemental analyses, IR spectra, single crystal X-ray diffraction and magnetic susceptibility measurements. Compound **6** exhibits mononuclear structure, **1–4** dinuclear structure whereas complex **5** yields two-dimensional sheets parallel to the (100) plane in which the deprotonated H_2L^4 act as bridging ligand. The magnetic study reveals dominating antiferromagnetic interactions in **1** and **5** whereas the ferromagnetic coupling dominates in **2–4**. The magnetic properties are interpreted in terms of the electronic structure of the Mn ions and structural parameters.

© 2013 Elsevier Ltd. All rights reserved.

1. Introduction

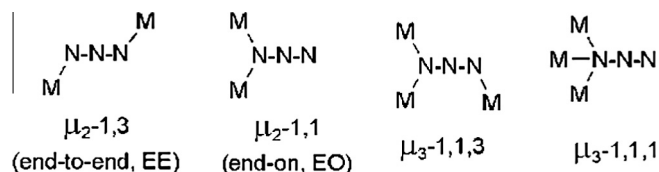
The study of poly-nuclear manganese complexes is of current interest due to the role they play in several redox systems such as in water oxidation in the active centre of Photosystem II [1] and in other redox-biochemical processes. Additionally, many manganese complexes possess large numbers of unpaired electrons, making them precursors for magnetic materials [2–5]. These findings have triggered the investigation of new molecular complexes based on manganese ions. In this context, dinuclear manganese Schiff base complexes are known to exhibit interesting magnetic properties [6,7] that can further be tailored towards assembly of molecule exhibiting single molecule magnet (SMM)

behavior. Due to the presence of energy barrier between spin-up and spin-down states, the SMMs may be potentially used as information storage at the molecular level. Moreover, these might be the unique systems for studying quantum spin tunnelling and quantum phase interference leading to their applications in molecular electronics too [8].

Among the bridging pseudohalide ions (N_3^- , NCS^- , NCO^-), the azide has been widely utilized not only as a versatile bridging ligand, but also as an excellent magnetic coupler [9]. When the azide anion acts as bridging ligand [10], it can bind metal ions in different coordination modes. The most common are the end-to-end (μ_2 -1,3- N_3 , EE) [11], and end-on (μ_2 -1,1- N_3 , EO) [12] modes, whereas triply μ_3 -1,1,1- N_3 [13], μ_3 -1,1,3- N_3 [14] quadruply μ_4 -1,1,1,1- N_3 [10] and μ_4 -1,1,3,3- N_3 [15] coordinated modes remain relatively rare (Scheme 1). In most cases the end-to-end ($\mu_{1,3}$) and end-on ($\mu_{1,1}$) coordination modes mediate antiferromagnetic and ferromagnetic interaction, respectively, but an increasing number of exceptions have been recently observed [16]. Hence, the

* Corresponding authors. Tel.: +98 241 5152576; fax: +98 241 5283203 (H. Hosseini-Monfared).

E-mail addresses: monfared@znu.ac.ir (H. Hosseini-Monfared), jsanchiz@ull.es (J. Sanchiz), milosz.siczek@chem.uni.wroc.pl (M. Siczek), radek.zboril@upol.cz (R. Zboril), pemay@cup.uni-muenchen.de (P. Mayer).



Scheme 1. The common metal ion bridging modes for azide ion illustrated by double-bridged μ_2 -1,3 (EE), μ_2 -1,1 (end-on, EO), triple-bridged μ_3 -1,1,3 and μ_3 -1,1,1.

synthesis, the structural characterization and the study of the magnetic properties of azide-containing complexes with different magnetic features is an emerging and substantial subject of scientific researches.

Acyl and aroyl hydrazones are a multipurpose class of ligands (Scheme 2) which have a range of biological and chemical activities. Hydrazones exhibit physiological and biological activities in the treatment of several diseases such as tuberculosis [17], Fe overload [18,19], and also as inhibitors for many enzymes [20]. Their metal complexes have also found applications in various physical and chemical processes e.g. non-linear optics, sensors, medicine [21] and, as well as non-symmetrical salens, can act as effective catalysts towards alkene epoxidation [22]. Moreover, they are of interest in the field of electrochromism where a change in the oxidation state of the metal is possible [23]. Acyl and aroyl hydrazones contain trigonal N- and O-donor atoms that can coordinate to metal ions [24] acting as bidentate [25], tridentate, tetradentate [26], or pentadentate ligands [27] depending on the nature of heterocyclic ring-substituents attached to the hydrazone unit. These ligands exhibit a facile keto–enol tautomerization which can modulate the coordination to the metal as a mono-negative or di-negative ligand in the keto or enol form, respectively.

Metal complexes with mixed ligands of hydrazone Schiff base and azide are rare [28], although combination of different properties

of azide and hydrazone Schiff base as ligands could be interesting. In this sense, there are only a few studies on azide as bridging [29] and non-bridging ligands between two Mn(III) ions [30,31]. And to the best of our knowledge, there is no report on the structure of Mn(II) hydrazone complexes with azide bridging ligands. Thus in order to improve the knowledge in this kind of compounds we report herein the structures, thermal stability and magnetic properties of mono-nuclear, dinuclear and polymeric Mn(II,III) complexes with mixed azide and aroyl hydrazone ligands (Scheme 2).

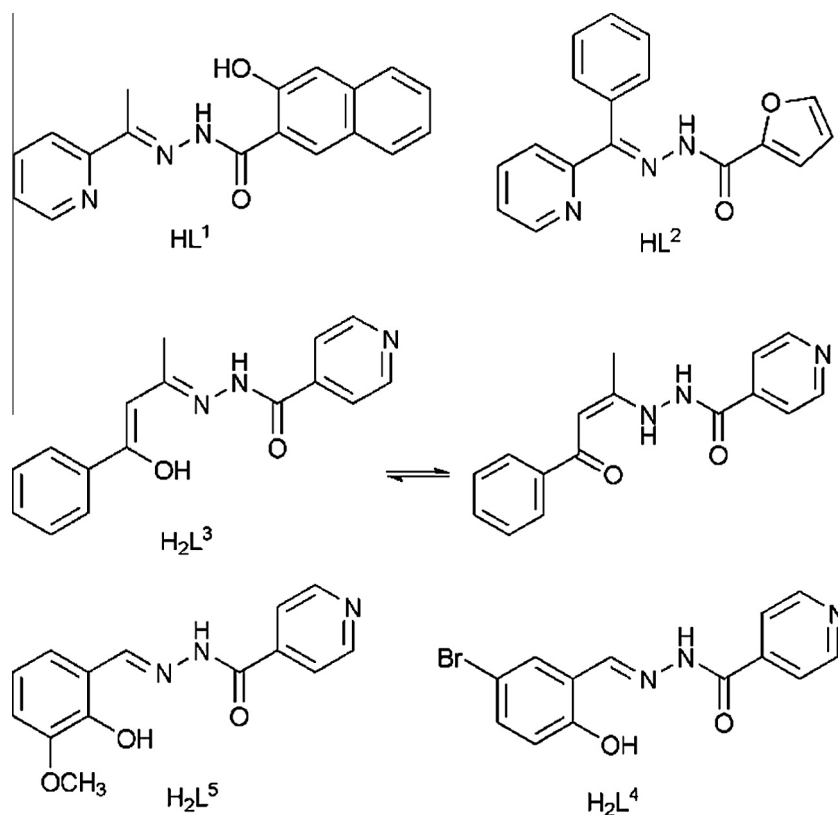
2. Experimental

2.1. Materials and instrumentations

Manganese(II) chloride tetrahydrate, sodium azide, 4-pyridine-carboxylic acid hydrazone, furane-2-carboxylic acid hydrazone, 3-hydroxy-2-naphthoic acid hydrazone, 5-bromo-2-hydroxybenzaldehyde, 2-hydroxy-3-methoxybenzaldehyde, 2-acetylpyridine, 2-benzoylpyridine, benzoylacetone and solvents were purchased from Merck and used as received. IR spectra were recorded in KBr disks with a Bruker FT-IR spectrophotometer. UV–Vis spectra of solutions were recorded on a thermo spectronic, Helios Alpha spectrometer. Elemental analyses were determined on a CHN Perkin–Elmer 2400 analyzer. The manganese content of the final material was determined by a Varian spectrometer AAS-110.

2.2. Synthesis of the ligands

General procedure: the ligands were prepared in a similar manner by refluxing a mixture of acid hydrazone (1.0 mmol) and appropriate aldehyde or ketone with equivalent molar ratio in 20 ml methanol for 6 h. The solution volume was decreased to 5 ml by removing the solvent and cooled to room temperature. The



Scheme 2. The aroylhydrazone ligands which used in the synthesis of complexes.

obtained solids were separated and filtered off, washed with cooled methanol and then dried in air. Completion of the reactions was checked by TLC on silica gel plates.

2.2.1. (*E*)-3-Hydroxy-*N'*-(1-(pyridin-2-yl)ethylidene)-2-naphthohydrazide (HL¹)

Yield: 87%. Color: light brown. M.p. >200 °C. *Anal. Calc.* for C₁₈H₁₅N₃O₂ (MW = 305.33 g/mol): C, 70.81; H, 4.95; N, 13.76. Found: C, 70.62; H, 4.87; N, 13.80%. ¹H NMR (250.13 MHz, DMSO-d₆, 25 °C, TMS): δ_H 11.79 (s, 1H, N-H), 11.66 (s, 1H, O-H), 8.64 (s, 1H), 8.15 (d, 1H, *J* = 8.00 Hz), 7.99 (d, 1H, *J* = 7.75 Hz), 7.88 (t, 1H, *J* = 7.5 Hz), 7.76 (d, 1H, *J* = 8.25 Hz), 7.50 (m, 4H), 7.34 (d, 1H, *J* = 8.00 Hz), 2.42 (s, 3H). ¹³C NMR (250.13 MHz, DMSO-d₆ + D₂O): δ_C 7.18–8.77 (10H- Aromatics), 2.60 (s, 3H) ppm. ¹³C NMR (62.90 MHz, DMSO-d₆): δ_C 12.3, 111.2, 120.9, 121.1, 124.4, 124.7, 126.2, 127.7, 128.8, 129.4, 133.0, 136.3, 137.2, 149.1, 154.0, 153.0, 155.3, 162.0. UV–Vis in CH₃OH [λ_{max}/nm, with ε (dm³ mol⁻¹ cm⁻¹)]: 228 (101 000), 311 (73 900), 366 (22 300^{sh}). IR data of the ligands and complexes are given in [Supplementary Information](#).

2.2.2. (*E*)-*N'*-(phenyl(pyridin-2-yl)methylene)furan-2-carbohydrazide (HL²)

Yield: 92%. Color: light brown. M.p. 122 °C. *Anal. Calc.* for C₁₇H₁₃N₃O₂ (MW = 291.30 g/mol): C, 70.09; H, 4.50; N, 14.42. Found: C, 70.14; H, 4.45; N, 14.53%. ¹H NMR (250.13 MHz, DMSO-d₆, 25 °C, TMS): δ_H 14.67 (s, 1H, CO-NH-), 9.73 (s, 1H), 8.92 (s, 1H), 8.10 (d, 1H, *J* = 6.75 Hz), 7.94 (m, 2H), 7.30–7.54 (m, 5H), 6.70 (d, 1H, *J* = 7.25 Hz) ppm. ¹³C NMR (62.90 MHz; DMSO-d₆): δ_C 112.9, 122.0, 124.6, 125.5, 126.7, 128.9, 129.3, 129.5, 131.7, 137.2, 137.8, 138.8, 146.7, 149.0, 149.3, 152.1, 155.3 ppm. UV–Vis in CH₃OH [λ_{max}/nm, with ε (dm³ mol⁻¹ cm⁻¹)]: 205 (40 600^{sh}), 272 (19 260), 315 (25 800).

2.2.3. (*E*)-*N'*-((*Z*)-4-hydroxy-4-phenylbut-3-en-2-ylidene)isonicotinohydrazide (H₂L³)

Yield: 89%. Color: colorless. M.p. 159 °C. *Anal. Calc.* for C₁₆H₁₅N₃O₂ (MW = 281.31 g/mol): C, 68.31; H, 5.37; N, 14.94. Found: C, 68.48; H, 5.32; N, 15.02%. ¹H NMR (250.13 MHz, DMSO-d₆, 25 °C, TMS): δ_H 12.28 (s, 1H), 11.14 (s, 1H), 8.77 (d, 2H, *J* = 4.75 Hz), 8.65 (s, 1H), 7.88 (d, 2H, *J* = 6.25 Hz), 7.78 (d, 2H, *J* = 7.25 Hz), 7.45 (m, 3H), 5.99 (s, 1H), 2.07 (s, 3H) ppm. ¹H NMR (250.13 MHz, DMSO-d₆ + D₂O): δ_H 7.72–8.72 (9H, aromatic), 5.95 (s, 1H), 2.03 (s, 3H) ppm. ¹³C NMR (62.90 MHz; DMSO-d₆): δ_C 16.1 (CH₃ of the first tautomer), 18.4 (CH₃ of the second tautomer), 92.3, 93.3, 121.9, 123.0, 125.0, 127.4, 127.7, 128.5, 128.8, 131.6, 139.3, 139.9, 143.5, 143.9, 150.0, 150.9, 156.3, 164.0, 164.7, 165.2 (Ph-C(OH)=, the second tautomer), 186.7 (the carbonyl of benzoyl, Ph-C(O)-, the first tautomer) ppm. UV–Vis in CH₃OH [λ_{max}/nm, with ε (dm³ mol⁻¹ cm⁻¹)]: 211 (25 920), 249 (16 780), 335 (10 500), 403 (8 640).

2.2.4. (*E*)-*N'*-(5-bromo-2-hydroxybenzylidene)isonicotinohydrazide (H₂L⁴)

Yield: 94%. Color: white. M.p. 286 °C. *Anal. Calc.* for C₁₃H₁₀BrN₃O₂ (MW = 320.14 g/mol): C, 48.77; H, 3.15; N, 13.13. Found: C, 48.70; H, 3.17; N, 13.09%. ¹H NMR (250.13 MHz, DMSO-d₆, 25 °C, TMS): δ_H 12.34 (s, 1H, CO-NH-), 11.13 (s, 1H, -OH), 8.76 (d, 2H, *J* = 4.25 Hz), 8.61 (s, 1H, -CH=N), 7.80 (m, 3H), 7.39 (d, 1H, *J* = 8.5 Hz), 6.87 (d, 1H, *J* = 8.5 Hz) ppm. ¹H NMR (250.13 MHz, DMSO-d₆ + D₂O): δ_H 8.56 (s, 1H, CH=N), 8.72 (7H, aromatics) ppm. ¹³C NMR (62.90 MHz; DMSO-d₆): δ_C 111.0, 119.1, 121.7, 130.6, 134.3, 140.3, 146.9, 150.0, 153.9, 156.9, 162.0 ppm. UV–Vis in CH₃OH [λ_{max}/nm, with ε (dm³ mol⁻¹ cm⁻¹)]: 220 (29 500), 246 (15 780^{sh}), 290 (19 800), 342 (14 160).

2.2.5. (*E*)-*N'*-(2-hydroxy-3-methoxybenzylidene)isonicotinohydrazide (H₂L⁵)

Yield: 90%. Color: white. M.p. 262 °C. *Anal. Calc.* for C₁₄H₁₃N₃O₃ (MW = 271.27 g/mol): C, 61.99; H, 4.83; N, 15.49. Found: C, 61.90; H, 4.79; N, 15.54%. ¹H NMR (250.13 MHz, DMSO-d₆, 25 °C, TMS): δ_H 12.25 (s, 1H, CO-NH-), 10.69 (s, 1H, -OH), 8.77 (d, 2H, *J* = 2.25 Hz), 8.67 (s, 1H, -CH=N), 7.81 (d, 2H, *J* = 2.25 Hz), 7.17 (d, 1H, *J* = 7.5 Hz), 7.02 (d, 1H, *J* = 7.5 Hz), 6.84 (t, 1H, *J* = 7.75 Hz), 3.79 (s, 3H, -OCH₃) ppm. ¹H NMR (250.13 MHz, DMSO-d₆ + D₂O): δ_H 8.58 (s, 1H, -CH=N), 6.83–8.70 (7H, aromatics), 3.74 (3H, OCH₃) ppm. ¹³C NMR (62.90 MHz; DMSO-d₆): δ_C 56.3, 114.4, 119.4, 119.6, 120.9, 122.1, 140.4, 147.6, 148.4, 149.3, 150.9, 161.8. UV–Vis in CH₃OH [λ_{max}/nm, with ε (dm³ mol⁻¹ cm⁻¹)]: 223 (23 940), 305 (20 020).

2.3. Synthesis of the complexes

Polycrystalline samples of the **1–4** complexes were obtained by the same method. The desired ligand (HL¹, HL², H₂L³ and H₂L⁴) (0.196 mmol) was dissolved in a mixed-solvent solution (methanol/ethanol 70:30 v/v, 30 ml) and to this solution MnCl₂·4H₂O (78 mg, 0.392 mmol) and NaN₃ (4 mg, 0.615 mmol) were added and then gently refluxed for 4 h. After cooling, the resulting solid was filtered off, washed with cooled absolute ethanol and dried at 100 °C. (*Caution!* Azido compounds of metal ions are potentially explosive and only a small amount of the materials should be prepared and handled with care).

Single crystals of the complexes were obtained by the reaction of MnCl₂·4H₂O (95 mg, 0.48 mmol), NaN₃ (47 mg, 0.723 mmol) and 0.24 mmol of the desired ligand which were placed in the main arm of a branched tube and a mixed solvent solution of methanol/ethanol (70:30 v/v) was added to fill the arms. The tube was sealed and the arm containing the reagents immersed in an oil bath at 60 °C while the other arm was kept at ambient temperature. After 5 days, crystals of **1–5** were deposited in the cooler arm, which were analyzed after separation and washing with methanol. The red complex [Mn₂(L⁴)₂(HOCH₃)₂]_n (**5**) was produced as minor product in the synthesis of complex **4**.

Compound **6** is obtained by refluxing H₂L⁵ (0.05, 0.178 mmol) and MnCl₂·4H₂O (70 mg, 0.355 mmol) in 10 ml ethanol for 4 h. Then filtered and washed with ethanol.

2.3.1. [Mn(L¹)(N₃)(OHCH₃)₂] (1)

Yield: 73%. Color: red–orange. *Anal. Calc.* for C₃₈H₃₆Mn₂N₁₂O₆ (MW = 866.67) C, 52.66; H, 4.19; N, 19.39; Mn, 12.68. Found: C, 52.70; H, 4.16; N, 19.46; Mn, 12.50%. UV–Vis in CH₃OH [λ_{max}/nm, with ε (dm³ mol⁻¹ cm⁻¹)]: 207 (93 750), 230 (72 900), 362 nm (47 000).

2.3.2. [Mn(L²)(N₃)(HOCH₃)₂·0.5(CH₄O)] (2)

Yield: 79%. Color: red–orange. *Anal. Calc.* for C₃₆H₃₂Mn₂N₁₂O₆ (MW = 854.64 g/mol): C, 51.30; H, 4.01; N, 19.67; Mn, 12.86. Found: C, 51.44; H, 3.96; N, 19.82; Mn, 12.97%. UV–Vis in CH₃OH [λ_{max}/nm, with ε (dm³ mol⁻¹ cm⁻¹)]: 205 (94 100), 261 (46 450), 290 (40 050^{sh}), 385 (86 000).

2.3.3. [Mn(L³)(N₃)(HOCH₃)_{0.75}(EtOH)_{0.25}] (3)

Yield: 76%. Color: black. *Anal. Calc.* for C_{34.50}H₃₅Mn₂N₁₂O₆ (MW = 823.62 g/mol): C, 50.31; H, 4.28; N, 20.41; Mn, 13.34. Found: C, 49.98; H, 4.23; N, 20.55; Mn, 14.00%. UV–Vis in CH₃OH [λ_{max}/nm, with ε (dm³ mol⁻¹ cm⁻¹)]: 231 (58 150), 270 (44 400), 336 (26 800), 431 (29 450).

2.3.4. [Mn(L⁴)(N₃)(OHCH₃)₂] (4)

Yield: 83%. Color: black. *Anal. Calc.* for C₂₈H₂₄Br₂Mn₂N₁₂O₆ (MW = 894.25) C, 37.61; H, 2.71; N, 18.80, Mn, 12.29. Found: C,

37.69; H, 2.70; N, 18.89; Mn, 12.15%. UV–Vis in CH₃OH [λ_{max} /nm, with ϵ (dm³ mol⁻¹ cm⁻¹): 236 (89800), 316 (48900), 417 nm (24850).

2.3.5. [Mn₂(L⁴)₂(OHCH₃)₂]_n (5)

Yield: 72%. Color: red–orange. Anal. Calc. for C₂₈H₂₄Br₂Mn₂N₆O₆ (MW = 810.21 g/mol): C, 41.51; H, 2.99; N, 10.37; Mn, 13.56. Found: C, 41.35; H, 3.02; N, 10.31; Mn, 13.45%. UV–Vis in CH₃OH [λ_{max} /nm, with ϵ (dm³ mol⁻¹ cm⁻¹): 227 (66500), 268 (41950^{sh}), 324 (28750), 406 (14600).

2.3.6. [Mn(H₂L⁵)₂(OHCH₂CH₃)Cl₂] (6)

Yield: 78%. Color: yellow. Anal. Calc. for C₃₂H₃₈Cl₂MnN₆O₈ (MW = 760.52 g/mol): C, 50.54; H, 5.04; N, 11.05; Mn, 7.22. Found: C, 50.40; H, 5.09; N, 11.13; Mn, 7.30%. UV–Vis in CH₃OH [λ_{max} /nm, with ϵ (dm³ mol⁻¹ cm⁻¹): 224 (75050), 307 (44650), 405 (12500).

2.4. X-ray diffraction data collection and refinement

Data collections for X-ray structure determination were performed on a KUMA KM4 CCD (1) and an Oxford Diffraction XCalibur (2, 3, 4, 5, 6) using Mo K α radiation (0.71073 Å) at low temperatures. The structures were solved by direct methods with SHELXS [32] or SIR97 [33], and refined with full-matrix least-squares technique on F² with SHELXL-97 [32]. The hydrogen atoms were calculated in idealized geometry riding on their parent atoms with the exception of the methanol-O-bonded hydrogen (located from difference maps). The disorder of the methanol molecule in 2 has been refined by a split model. The O-bonded hydrogen atoms were located from the difference maps and refined with constraints. The

structure plots were prepared with DIAMOND [34]. The crystal data and refinement parameters are presented in Table 1.

2.5. Magnetic measurement

Magnetic susceptibility measurements on polycrystalline samples were carried out by means of a Quantum Design SQUID MPMS XL magnetometer. The *dc* measurements were performed in the temperature range 1.9–300 K at applied magnetic fields of 1000 Oe. *ac* measurements were performed in the 2–5 K range under a *dc* field of 0 Oe and an *ac* field of 3.5 Oe. Diamagnetic corrections of the constituent atoms were estimated from Pascal's constants [2] and experimental susceptibilities were also corrected for the temperature-independent paramagnetism and the magnetization of the sample holder.

3. Results and discussion

3.1. Syntheses of complexes and spectroscopy

The ligands were prepared in methanol following the reported method [22]. The reaction of aromatic acid hydrazides with favored aldehyde/ketones containing N/O donor atom in suitable position gave the desired tridentate Schiff base ligands in excellent yields and purity which are shown in Scheme 2. The analytical and spectroscopic data confirmed the syntheses of the ligands. ¹H NMR, ¹³C NMR and IR spectroscopy confirmed that aroylhydrazone moiety of the ligands are in keto-form in solution and solid state. Furthermore, the ¹³C NMR spectrum of ligand H₂L³ proved the existence of two tautomeric forms which are in equilibrium

Table 1
Parameters of data collection and structure refinement of 1–6.

	1	2	3	4	5	6
Net formula	C ₃₈ H ₃₆ Mn ₂ N ₁₂ O ₆	C ₃₆ H ₃₂ Mn ₂ N ₁₂ O ₆ ·0.5(CH ₄ O)	C _{34.50} H ₃₅ Mn ₂ N ₁₂ O ₆	C ₂₈ H ₂₄ Br ₂ Mn ₂ N ₁₂ O ₆	C ₂₈ H ₂₄ Br ₂ Mn ₂ N ₆ O ₆	C ₃₂ H ₃₈ Cl ₂ MnN ₆ O ₈
<i>M_r</i> (g mol ⁻¹)	866.67	854.64	823.62	894.252	810.211	760.52
Crystal size (mm)	0.26 × 0.20 × 0.18	0.22 × 0.15 × 0.11	0.46 × 0.32 × 0.26	0.19 × 0.12 × 0.03	0.15 × 0.13 × 0.12	0.20 × 0.17 × 0.10
<i>T</i> (K)	100 (2)	90 (2)	100 (2)	100(2)	173(2)	100
Diffractometer	KUMA KM4 CCD	Xcalibur PX	Xcalibur PX	'OxfordXCalibur'	'OxfordXCalibur'	Oxford Xcalibur
Crystal system	monoclinic	triclinic	monoclinic	triclinic	monoclinic	triclinic
Space group	<i>P</i> 2 ₁ / <i>c</i>	<i>P</i> 1	<i>P</i> 2 ₁ / <i>n</i>	<i>P</i> 1	<i>C</i> 2/ <i>c</i>	<i>P</i> 1
<i>a</i> (Å)	11.451 (4)	9.736 (4)	9.955 (3)	7.9733 (5)	16.3851 (10)	8.222 (3)
<i>b</i> (Å)	7.851 (2)	12.988 (5)	17.603 (6)	10.0811 (7)	13.6703 (5)	8.918 (3)
<i>c</i> (Å)	22.101 (7)	17.104 (7)	11.531 (4)	10.5840 (5)	17.7092 (15)	12.458 (4)
α (°)		73.08 (4)		98.814 (5)	90	69.33 (5)
β (°)	101.66 (3)	75.49 (4)	114.10 (5)	98.786 (5)	129.237 (4)	89.78 (5)
γ (°)		70.89 (5)		93.320 (5)	90	74.71 (5)
<i>V</i> (Å ³)	1945.9 (10)	1926.1 (13)	1844.5 (13)	827.94 (9)	3072.3 (3)	820.4 (5)
<i>Z</i>	2	2	2	1	4	1
Calc. density (g cm ⁻³)	1.479	1.474	1.483	1.79356(19)	1.75166(17)	1.539
μ (mm ⁻¹)	0.71	0.72	0.75	3.238	3.475	0.63
Absorption correction	analytical	analytical	analytical	'multi-scan'	'multi-scan'	analytical
Transmission factor range	0.866, 0.912	0.878, 0.925	0.762, 0.839	0.86623–1.00000	0.92214–1.00000	0.873–0.944
Refls. measured	31102	22371	14776	6278	11836	14463
<i>R</i> _{int}	0.034	0.028	0.019	0.0392	0.0416	0.045
θ range	2.8–36.9	2.4–35	2.5–29	4.14–26.33	4.21–26.35	2.5–34.1
Observed refls.	6109	8815	4005	1936	1983	4549
<i>X</i> , <i>y</i> (weighting scheme)	0.039, 0	0.052, 0	0.043, 0.273	0.0195, 0	0.0349, 0	0.064, 0
Hydrogen refinement	geom.	geom.	geom.	mixed	mixed	geom.
Reflections in refinement	9119	12848	4670	3354	3121	6662
Parameters	265	557	257	231	204	225
Restraints	0	0	2	1	0	0
<i>R</i> (<i>F</i> _{obs})	0.037	0.041	0.026	0.0372	0.0323	0.046
<i>R</i> _w (<i>F</i> ²)	0.081	0.104	0.074	0.0629	0.0713	0.119
<i>S</i>	1.01	1.02	1.09	0.788	0.876	1.01
Shift/error _{max}	0.002	0.001	0.001	0.001	0.001	0.001
Max/min electron density (e Å ⁻³)	0.54/–0.26	0.97/–0.31	0.37/–0.27	0.805/–0.379	0.808/–0.442	1.12/–1.15

in the solution; it shows 23 resonances, while the ligand contains only 16 carbon atoms (see Section 2).

One-pot synthesis of 1:2:3 molar ratio of aroylhydrazone (HL¹, HL², H₂L³, H₂L⁴), manganese(II) chloride tetrahydrate and NaN₃ in methanol/ethanol (70:30 v/v) afforded hexacoordinated dinuclear compounds of [Mn(L¹)(N₃)(HOCH₃)₂]₂ (**1**), [Mn(L²)(N₃)(HOCH₃)₂]₂ (**2**), [Mn(HL³)(N₃)(HOCH₃)_{0.75}(EtOH)_{0.25}]₂ (**3**) and [Mn(L⁴)(N₃)(HOCH₃)₂]₂ (**4**), respectively. All complexes have been isolated in good yield and micro analytical data are consistent with the compositions proposed. The products in cases **3** and **4** contain manganese(III) rather than manganese(II), as in the starting materials, due to aerial oxidation that occurs spontaneously in the reaction mixture. Other workers have reported similar observations [35,36]. The coordination polymer [Mn₂(L⁴)₂(HOCH₃)₂]_n (**5**) was produced as the minor product in the synthesis of complex **4**. However, the reaction of H₂L⁴, MnCl₂·4H₂O and NaN₃ with molar ratios of 1:2:0.4 in methanol/ethanol produced merely compound **5**. The presence of sodium azide to synthesis compound **5** is essential; in the absence of NaN₃, the solution of H₂L⁴ and MnCl₂·4H₂O at 60 °C remained without any change even after one month, but after the addition of NaN₃ the solution color changed and **5** was formed immediately. Ligand H₂L⁵ was treated with MnCl₂·4H₂O in the absence of NaN₃ with expectation to get a coordination polymer similar to **5**, but the mononuclear Mn(II) complex **6** was produced in which two H₂L⁵ without deprotonation and two ethanol molecules are coordinated to the Mn centre in addition to the two chloride ligands. Moreover, replacing Mn(NO₃)₂·4H₂O by MnCl₂·4H₂O in the reaction with a similar ligand (isonicotinoylhydrazone) produced the nitrated ligand without any complex formation [37]. The typical syntheses of **1–6** are summarized in Scheme 3.

The compounds were characterized using microanalyses, spectroscopic and thermal studies. The microanalytical results are in good agreement with formulations **1–6**. The air-stable compounds are soluble in a wide range of common organic solvents such as methanol, acetonitrile, dimethylformamide, dimethylsulfoxide, but are insoluble in water. Selected stretching frequencies of the ligands and their complexes are summarized in Table 2. In IR spectra, the stretching vibrations of azide ion in **1–4** are seen as strong ν_{as}(N₃) absorptions at about 2065 cm⁻¹. The peaks above approximately 2055 cm⁻¹ indicate μ_{1,1} bridging mode of azides [38]. In the IR spectra, the hydrazone ligands show stretching bands attributed to N–H, C=O and C=N in the range 3134–3263, 1645–1690 and 1552–1603 cm⁻¹, respectively (Table 2) [26,39]. The presence of ν(OH) in HL¹ and H₂L^{3–5} as a weak band at about 3400 cm⁻¹ suggests an intramolecular hydrogen bonding (O–H...N) in these ligands [40]. The band at about 1250 cm⁻¹ is attributed to ν(C–O) (phenolic) stretching in the ligands H₂L⁵ and H₂L⁶ [41]. On complexation the absence of N–H and carbonyl bands, shifts in azomethine (–C=N–) band and appearance of >C=N–N=C< band support the coordination of the hydrazone ligands in the enol form as monoanionic {(L¹)⁻, (L²)⁻} in complexes **1** and **2** and dianionic {(L³)²⁻, (L⁴)²⁻} in complexes **3–5** (Scheme 3). Appearance of a broad peak at 3227 cm⁻¹ in **1** can be ascribed to the persistence

of an intramolecular hydrogen bond between O–H from naphthyl ring and of amide group nitrogen in enol form. The disappearance of the bands at 1266 cm⁻¹ (H₂L⁴) in complexes **4** and **5** show the involvement of phenolic oxygen in coordination through deprotonation. In complex **6** the stretching bands related to functional groups O–H, N–H, C=O and C=N are almost the same with that of H₂L⁵ (Table 2) hence the hydrazone ligand H₂L⁵ coordinate as a neutral monodentate ligand. Additionally, the appearance of very broad band at around 3400 cm⁻¹ can be related to the coordinated methanol (in **1–5**) or ethanol (in **3, 6**) to the manganese center [42,43].

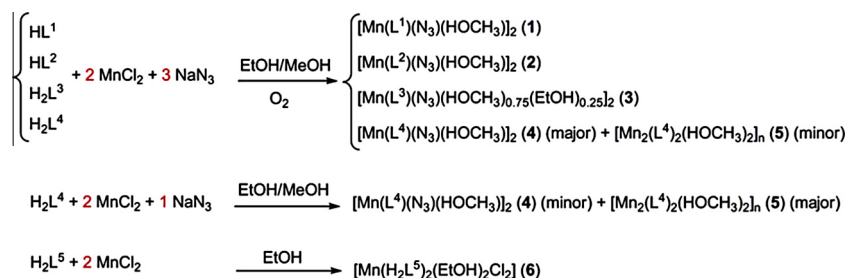
In methanol solutions, HL¹, HL², H₂L³ and H₂L⁴ show absorption maxima in the region 205–238 nm and 249–403 nm (Table S1). Based on their extinction coefficients these are assigned as due to π → π* and n → π* transitions, respectively. The corresponding Mn(II) and Mn(III) compounds **1–4** exhibit bands at λ_{max} values in the region 230–236 nm and 261–417 nm which are assignable to ligand-based π → π* and n → π* transitions, respectively. All bands shifts in complexes indicate the coordination of ligands to the metal ions. The bands appeared at about 405 nm for complexes **5/6** correspond to MLCT band which is absent in the ligands H₂L⁴ and H₂L⁵.

3.2. Thermal analyses

To examine thermal stabilities of **1, 3** and **5**, thermogravimetric and differential thermal analyses (TG–DTA) were made between 30 and 700 °C in the static atmosphere of nitrogen. TG curve (Fig. S7) shows that **1** is stable up to 129 °C, where the CH₃OH molecule is removed (observed 7.8, calcd. 7.5%) between 130 and 163 °C, then at 220 °C the N₃⁻ is removed (observed 10.6, calcd. 10.5%). At 410 °C the remaining organic aroylhydrazone ligand is lost (observed 35.4, calcd. 36.3%). TG curve of **3** (Fig. S8) shows that it loses CH₃OH at 144 °C (observed 6.5%, calcd. 7.6%), then at 232 °C the azide is lost (observed 10.5%, calcd. 11.4%). Finally aroylhydrazone L³ is removed during two steps at 341 and 407 °C (observed 30.0%, calcd. 31.7%). A first TG step of complex **5** (Fig. S9) derives from the methanol loss of the sample at 118 °C (observed 4.8%, calcd. 7.9%). The remaining organic ligand L⁴ is removed during two steps (at 372 °C, Δm ≈ -1.7% and at 423 °C, Δm ≈ -29.3%) which results to total mass loss of CH₃OH (calcd. 7.9%) + L⁴ (calcd. 57.9%) to yield the overall mass loss of Δm ≈ -65.3% (calcd. 65.8%) up to 840 °C. For the studied complexes, the final product is estimated to be Mn₂O₃.

3.3. Crystal structures of [Mn(L¹)(N₃)(HOCH₃)₂]₂ (**1**) and [Mn(L²)(N₃)(HOCH₃)₂]₂ (**2**)

The structural analyses reveal that **1–4** comprise of dinuclear units containing double μ_{1,1}-N₃ bridges, whereas **5** forms a 2D coordination polymer and **6** is a mononuclear Mn(II) complex. Selected bond distances and angles are listed in Table S2 of the Supplementary information section. The structures of **1–4** are built



Scheme 3. Reactions of the aroylhydrazone Schiff base ligands (Scheme 2) and MnCl₂·4H₂O with NaN₃ to give (b) compounds **1–6**.

Table 2
Selected characteristic IR bands of the ligands (HL¹⁻², H₂L³⁻⁵) and complexes **1-6**.

Comp.	$\nu(\text{O-H})$	$\nu(\text{N-H})$	$\nu(\text{C=O})$	$\nu(\text{C=N})$	$\nu(\text{N}_3)$
HL ¹	3445 (w, br)	3263 (m)	1645 (vs)	1552 (s)	
HL ²	–	3140 (m)	1683 (vs)	1585 (vs)	
H ₂ L ³	3472 (w, br)	3134 (m)	1689 (vs)	1593 (m)	
H ₂ L ⁴	3417 (w, br)	3141 (m)	1675 (vs)	1615 (m)	
H ₂ L ⁵	3445 (w, br)	3202 (m)	1690 (vs)	1602 (s)	
1	3381 (w)	3227 (m,br)	1630 (m)	1595 (m)	2066 (vs)
2	3597 (w) 3384 (w, br)	–	–	1582 (m)	2065 (vs)
3	3761 (w) 3451 (w,vbr)	–	–	1636 (w)	2069 (vs)
4	3382 (w, br)	–	–	1594 (s)	2063 (vs)
5	3431 (m, vbr)	–	–	1602 (vs)	
6	3458 (s)	3199 (m)	1677 (vs)	1609 (m)	

up of neutral dinuclear units. In **1** and **2** the two manganese(II) centres are bridged by two $\mu_{1,1}\text{-N}_3$ to form a planar four membered Mn–($\mu_{1,1}\text{-N}_3$)₂–Mn ring. The overall geometry around each manganese(II) in complexes **1** and **2** is best described as a distorted octahedron with an MnN₄O₂ chromophores (Figs. 1 and 2). Compound **2** exhibits two crystallographically independent molecules (described as **2A** and **2B**). Overlay of this two molecules show that they are almost identical (Fig. S10), and in the following description only molecule **2A** will be discussed. The aroylhydrazone Schiff base ligand forms a basal plane (equatorial plane) together with the nitrogen atom from the azide bridging ligand. An axial position is occupied by the oxygen atom from methanol and another axial position is occupied by the nitrogen atom from the second azide bridging ligand. In both the cases, each manganese(II) center deviates 0.104(1) Å in **1** and 0.125(1) Å in **2A** from the mean plane N1/N2/O1/N4 towards the methanol. Mn–N bond distances are in the range 2.1506(11)–2.3109(10) Å for **1** and 2.170(2)–2.3146(18) Å for **2A**. The Mn–O and Mn–N distances are close to those found in other octahedral Mn(II) complexes with N₂O-donor hydrazone ligand [22,44]. The axial Mn–Nⁱ ($i = 1 - x, 1 - y, 1 - z$) bond of 2.3109(10) Å is longer than equatorial azide Mn–N₄ distance of 2.1506(11) Å. This is thus an example of an asymmetric EO doubly bridged Mn–azide. The degrees of distortion from ideal octahedral geometry are reflected in *cisoid* [71.32(4)–118.83(4)° in **1** and 70.54(7)–113.97(7)° in **2A**] and *transoid* [143.67(4)–173.32(3)° in **1** and 141.97(6)–170.75(5)° in **2A**] bond angles; the N₄–Mn–Nⁱ (in **1**) and N_{4A}–Mn¹–Nⁱ (in **2A**) bridging angles are 81.69(4)° and 78.80(7)°, respectively.

In this dimeric unit the Mn···Mn distance within the four-membered Mn₂N₂ cyclic units is 3.3766(11) Å in **1** and 3.4410(15) Å in **2A**. The four-membered Mn₂($\mu_{1,1}\text{-N}_3$)₂ cyclic units are planar, as is usual for the double end-on bridges [45]. The N_{azide}–Mn–N'_{azide} and Mn–N_{azide}–Mn' bond angles are respectively 81.69(4)°/98.31(4)° in **1** and 78.80(7)°/101.20(7)° in **2A** and are

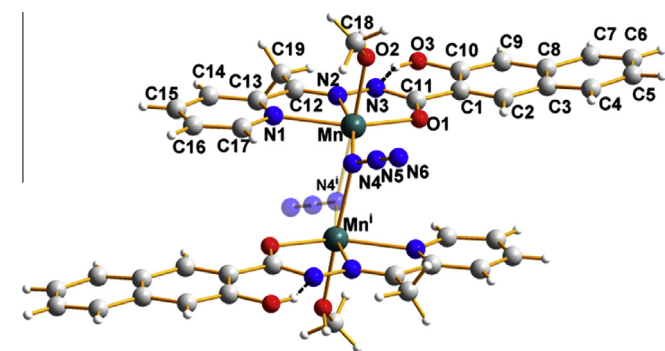


Fig. 1. Molecular structure of dinuclear [Mn(L¹)(N₃)(HOCH₃)₂] (**1**); symmetry transformation: $i = 1 - x, 1 - y, 1 - z$. Intramolecular hydrogen bonds are shown as dashed lines.

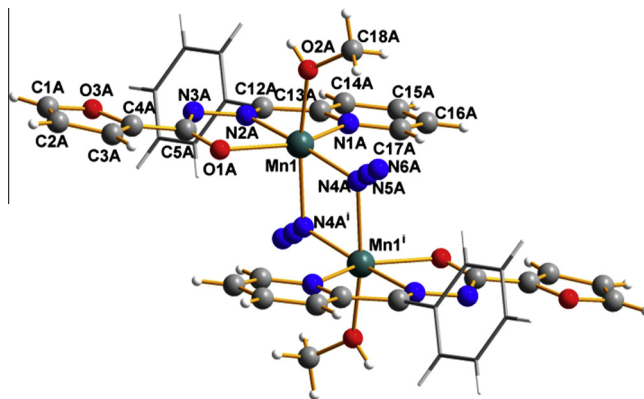


Fig. 2. Molecular structure of [Mn(L²)(N₃)(HOCH₃)₂] (**2A**); symmetry transformation $i = 2 - x, 2 - y, -z$.

very close to those observed in other reported azide bridged manganese complexes [45]. In Mn–($\mu_{1,1}\text{-N}_3$)₂–Mn linkage, the end-on azide group (N₄–N₅ bond) is not coplanar with the four-membered Mn₂N₂ cyclic unit and makes an angle of 27.01(6)° in **1** and 24.36(12)° in **2A**. The end-on azido bridges show asymmetric N–N distances (N₄–N₅/N₅–N₆) of 1.2088(12)/1.1548(13) Å and the N₄–N₅–N₆ angle is 177.62(12)° in **1** which is in usual manner for azide ligand [46].

It is worth mention that there is a strong intramolecular O–H···N hydrogen bond in complex **1** which effects on the keto–enol tautomerism (Table 2). Comparing the orientation of the hydrogen of the naphthol group (O–H) in free ligand with coordinated ligand to metal ions, indicates that the hydrogen of the hydroxy group in naphthol orients towards the outside of molecule in free ligands and takes part in intermolecular hydrogen bonding [47,48], whereas this hydrogen prefers inside orientation and participates in intramolecular hydrogen bonding in complex. This hydrogen bond prevents the tautomerism. N₃–C₁₁ and C₁₁–O₁ bond lengths in the naphthohydrazone are 1.3468(14) and 1.2701(13) Å, respectively, and are comparable to similar bond lengths in other reported hydrazone complexes which are about 1.31 and 1.30 Å for coordinated ligand in enol form [49] while in coordinated ligands in keto form are about 1.35 and 1.25 Å [22,44]. These finding together with the IR spectrum (slight decrease in $\nu(\text{C=O})$) show that the hydrogen atom of –NH–C=O has eliminated during the complexation and ligand coordinated in keto form.

Adjacent molecules of **1** are connected together by O–H···O hydrogen bonding which leads to infinite hydrogen-bonded 1D chains (Fig. S11, Table S4). Similar motifs can be also found in the structure **2** where **2A** and **2B** molecules create separately infinite hydrogen-bonded 1D chains. The molecules of solvated methanol are hydrogen bonded to chains of **2B**.

3.4. X-ray structures of [Mn(L³)(N₃)(HOCH₃)_{0.75}(EtOH)_{0.25}]₂ (**3**) and [Mn(L⁴)(N₃)(HOCH₃)₂] (**4**)

The manganese atoms have distorted octahedral geometry involving an N₃O₃ donor set. Complexes **3** and **4** (Figs. 3 and 4) consist of $\mu_{1,1}$ -azido-bridged dinuclear centrosymmetric molecules in which the Mn^{III} ions are in an axially elongated octahedral geometry. Each metal atom is coordinated in the equatorial coordination plane by N₂O₂ donor atoms from the tridentate hydrazone ligand (L³)²⁻ in **3** and (L⁴)²⁻ in **4** and one azido atom. Two axial positions are occupied by an oxygen atom of methanol (ethanol) and a nitrogen atom of another azido anion with longer distances. The axially coordinated methanol molecules are hydrogen-bonded to the pyridyl group of an adjacent dimeric unit in **3** and **4**

$[O2M \cdots N1^{ii} = 2.684(9) \text{ \AA}$ ($ii = 1 + x, y, z$) in $3/O3 \cdots N3^i = 2.723(4) \text{ \AA}$ ($i = x, -1 + y, z$) in **4**] to form a one-dimensional chain (Fig. S12 and Table S4). The bond lengths and bonding angles are as expected for other reported similar Mn complexes and agree with the coordination of hydrazone ligand in the enol form [49].

3.5. X-ray structure of $[Mn_2(L^2)_2(HOCH_3)_2]_n$ (**5**)

Fig. 5 shows the coordination diagram of **5** and it displays that the Mn(II) atom is coordinated by the atoms $O1_{phenol}$, $N2_{imine}$, $O2_{enol}$, $N3^{py}$, $O1^i_{phenol}$ and $O3$, which belong to three different symmetrically dependent doubly deprotonated (L^4)²⁻ anions and a CH_3OH molecule. The data (Table S2) indicate that the coordination sphere of the Mn1 atom is a distorted octahedron. Fig. 5 also displays that the atoms $O1$ and $O1^i$ act as bridging atoms between two Mn(II) ions with a $Mn1 \cdots Mn1^i$ distance of $3.3740(2) \text{ \AA}$, which creates a coplanar four-membered centrosymmetric ring. From Fig. 5 it can be derived that a doubly deprotonated (L^4)²⁻ anion acts as a tetradentate bridging ligand which is bound to three different Mn atoms through its three $O1_{phenol}/N2_{imine}/O2_{enol}$ atoms and a pyridyl nitrogen ($N3_{py}$) atom. In this coordination mode a two-dimensional sheet structure parallel to $[010]$ was fabricated as shown in Fig. S13. In the crystal there is one kind of hydrogen bonds (Table S4). The hydrogen bonds $O3-H \cdots N2^i$ and $N2 \cdots H-O3^i$ (symmetry code $i: 1 - x, y, 0.5 - z$) lead to a connection of adjacent sheets and the formation of a supramolecular three-dimensional structure as shown in Fig. S14.

3.6. X-ray structure of $[Mn(H_2L^5)_2(EtOH)_2Cl_2]$ (**6**)

In complex **6** the manganese atom sits on an inversion center leading to the *trans*-configuration of the two chloro, ethanol and H_2L^5 ligands (Fig. 6). With a length of $>29.17 \text{ \AA}$ along the H_2L^5 -Mn- H_2L^5 axis the metal-complex of *trans*- $[Mn(H_2L^5)_2(OHCH_2CH_3)_2Cl_2]$ (**6**) is one of the longest and anisotropic complex (aspect ratio 29.17:9.08:4.99) observed so far in Mn-arylohydrazone complexes. H_2L^5 coordinates as neutral ligand without deprotonation in the expected *trans*-C=N-N-C conformation and hydrogen bonding from the phenolic OH to the azomethine nitrogen atom. The phenyl and pyridyl rings are in plane with the central hydrazone moiety. Adjacent molecules are hydrogen bonded through the coordinated ethanol molecules and form a 1D supramolecule (Table S4, Fig. S15).

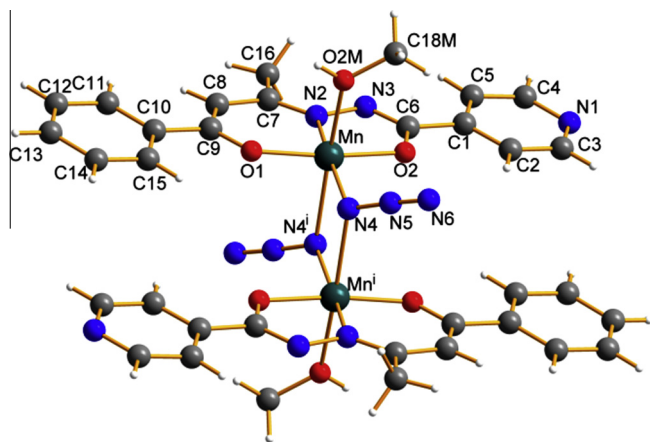


Fig. 3. Molecular structure of compound $[Mn(L^3)(N_3)(OHCH_3)_{0.75}(EtOH)_{0.25}]_2$ (**3**) with atom numbering; the major molecule (75% occupancy) of the disordered axial ligand ($\{CH_3OH\}$) is shown, the minor molecule (not shown) is CH_3CH_2OH with 25% occupancy. Bond lengths and angles are given in Table S2. Symmetry transformation $i = 1 - x, 1 - y, 1 - z$.

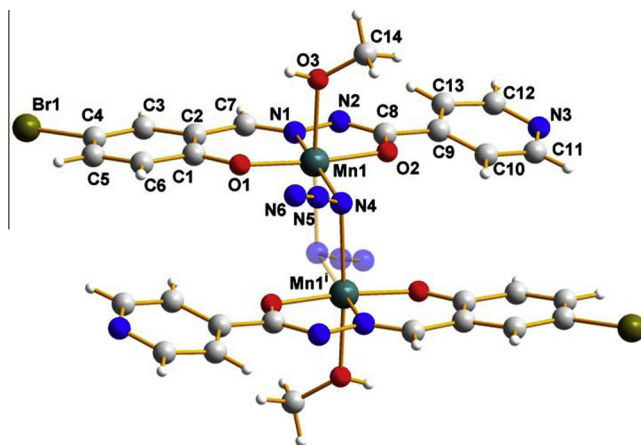


Fig. 4. Dimeric unit of compound $[Mn(L^4)(N_3)(HOCH_3)_2]_2$ (**4**) with atom numbering; symmetry transformation $i = 2 - x, -y, 2 - z$.

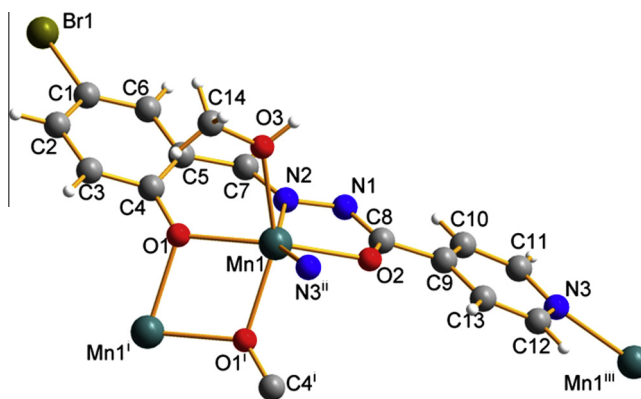


Fig. 5. Diagram of complex $[Mn_2(L^4)_2(OHCH_3)_2]_n$ (**5**) with the atom numbering scheme. For clarity the ligands on $N3^i$ have not been completed. The structure is polymeric; symmetry transformations: $i = 1 - x, -y, 1 - z$; $ii = 0.5 + x, -0.5 - y, 0.5 + z$; $iii = -0.5 + x, -0.5 - y, -0.5 + z$.

3.7. Magnetic properties

The temperature dependence of the $\chi_M T$ product for complexes **1** and **2** is shown in Fig. 7. In these compounds the manganese is on +2 oxidation state. At room temperature the $\chi_M T$ values for **1** are somewhat lower than those expected for two isolated Mn(II) ions (expected $\chi_M T = 4.375 \text{ cm}^3 \text{ mol}^{-1} \text{ K}$ per Mn(II) with $g = 2.00$ and $S = 5/2$). Upon cooling $\chi_M T$ continuously decreases to reach a value of $4.38 \text{ cm}^3 \text{ mol}^{-1} \text{ K}$ at 2 K. This behavior is indicative of the occurrence of weak antiferromagnetic interactions between the Mn(II) ions in **1**. On the other hand the values observed for the $\chi_M T$ product of **2** at room temperature are higher than those expected for two isolated Mn(II) ions and continuously increase on lowering the temperature to reach a value of $15.0 \text{ cm}^3 \text{ mol}^{-1} \text{ K}$ at 2 K. This value corresponds to a total spin of $S = 5$ [$\chi_M T = 3(N\beta^2 g^2 / 3kT) S(S + 1) = 15.0 \text{ cm}^3 \text{ mol}^{-1} \text{ K}$ for $g = 2.0$ and $S = 5$].

This behavior is indicative of the occurrence of a ferromagnetic coupling between the Mn(II) ions which ends up with a complete parallel alignment of the spins in the dinuclear units. The structure of both compounds consist of Mn(II) dimers and the magnetic susceptibility data have been analyzed by means of the corresponding expression for the magnetic susceptibility (1) derived from the Hamiltonian (2) [2]

$$\chi_M = \frac{2Ng^2\beta^2 e^x + 5e^{3x} + 14e^{6x} + 30e^{10x} + 55e^{15x}}{K(T - \Theta)1 + 3e^x + 5e^{3x} + 7e^{6x} + 9e^{10x} + 11e^{15x}} \quad (1)$$

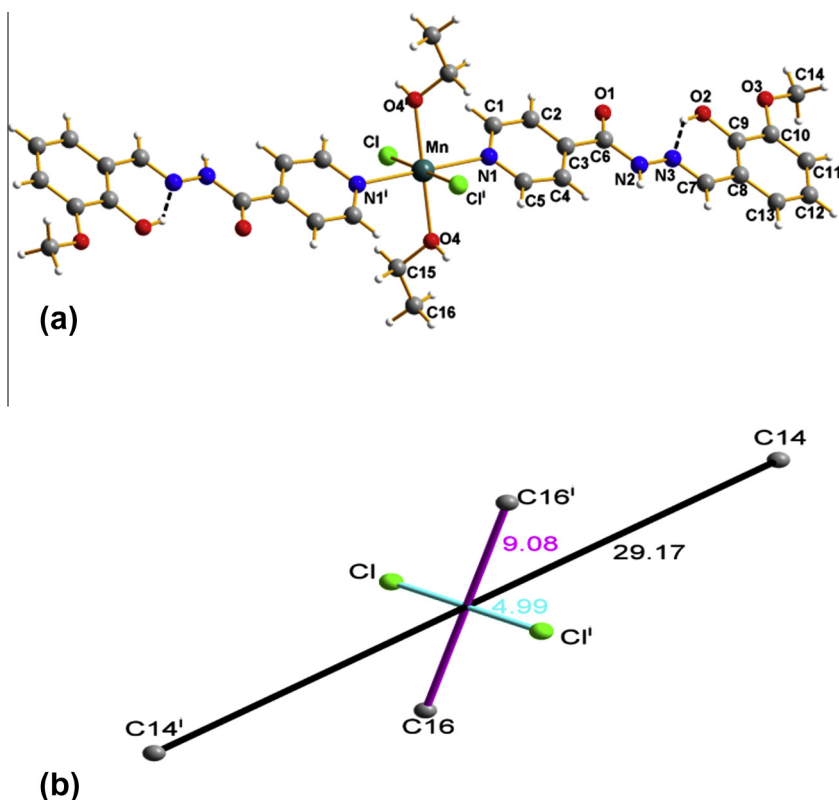


Fig. 6. (a) Molecular structure of $[\text{Mn}(\text{H}_2\text{L}^5)_2(\text{OHCH}_2\text{CH}_3)_2\text{Cl}_2]$ (**6**) and (b) complex with outer dimensions; symmetry transformation $i = 1 - x, 1 - y, 1 - z$.

$$\hat{H} = -J\hat{S}_1\hat{S}_2 + g\beta H\hat{S} \quad (2)$$

Where N stands for the Avogadro's number, β the Bohr magneton, k the Boltzmann constant, g the Landé factor, $x = J/kT$ and J the magnetic coupling constant. A Weiss-like parameter Θ , has been introduced to take into account interactions among the dinuclear units in **2**. Best fit parameters to Eq. (1) are $g = 1.96(1)$, $J = -0.12(1) \text{ cm}^{-1}$, $R = 8.62 \times 10^{-5}$ and $g = 2.02(1)$, $J = 1.94(2) \text{ cm}^{-1}$, $\Theta = -0.05(1) \text{ K}$, $R = 2.35 \times 10^{-5}$ for **1** and **2**, respectively. [R is the agreement factor defined as $\sum_i |(\chi_M T)_{\text{obs}}(i) - (\chi_M T)_{\text{calc}}(i)|^2 / \sum_i |(\chi_M T)_{\text{obs}}(i)|^2$]. The calculated curves match very well the experimental data in the whole temperature range as can be seen in Fig. 7.

In general the magnetic coupling constant can be expressed as the sum of two contributions, a ferromagnetic and an antiferromagnetic one $J = J_F + J_{AF}$ [2]. The magnetic coupling in EO azido-bridged Mn(II) dinuclear complexes is dominated by the spin polarization mechanism, in which the electron on a bridging nitrogen has opposite orientation than those of the Mn(II) ions favoring a ferromagnetic interaction between the metallic ions [50]. Theoretical studies have shown that the magnetic coupling constant increase with the Mn–N–Mn bridging angle (θ) with a cross-over from antiferro- to ferromagnetic coupling around 98° . For angles smaller than 98° an antiferromagnetic coupling is predicted whereas for angles larger than 98° a ferromagnetic one is expected [45]. Even, an equation has been proposed for the J – θ relationship, $J = 0.276 \theta - 26.9 \text{ (cm}^{-1}\text{)}$, however, this equation may be taken with care since it is an important simplification of the behavior and must be considered as an indication of the trend more than a tool to calculate the values of the magnetic coupling constants [45b,45c]. In the case of compound **1**, which displays a Mn–N–Mn angle of 98.31° , the antiferromagnetic contribution dominates with $J = -0.12 \text{ cm}^{-1}$ although a value of $J = 0.23 \text{ cm}^{-1}$ is predicted. Whereas, for compound **2** with a Mn–N–Mn angle of 100.88° the ferromagnetic one dominates with a predicted value of

$J = 0.94 \text{ cm}^{-1}$. Nevertheless, the predicted values are very close to those calculated from the magnetic susceptibility data.

Figs. 8 and 9 show the temperature dependence of the $\chi_M T$ product [χ_M is the magnetic susceptibility per two Mn(III) ions] which exhibit room temperature values of 6.01 and $6.10 \text{ cm}^3 \text{ mol}^{-1} \text{ K}$, for **3** and **4** respectively. These values are consistent with two non-interacting, or weakly interacting, high spin Mn(III) ions (a value of $\chi_M T = 6.00 \text{ cm}^3 \text{ mol}^{-1} \text{ K}$ is expected for two high spin Mn(III) ions in the spin-only model with $S = 2$ and $g = 2.00$) [2]. On lowering the temperature, compound **3** exhibits a continuous increase on the $\chi_M T$ product reaching a maximum value of $6.45 \text{ cm}^3 \text{ mol}^{-1} \text{ K}$. Also, compound **4** displays a continuous increase of the $\chi_M T$ product reaching a higher value ($9.0 \text{ cm}^3 \text{ mol}^{-1} \text{ K}$ at 7 K) and then decreasing at lower temperatures. Both compounds show a ferromagnetic coupling between the Mn(III) ions, but the coupling is somewhat stronger in **4** since the $\chi_M T$ product reaches higher values. The decrease of the $\chi_M T$ product at low temperatures, shown by **4**, occurs due to single ion zero-field-splitting and/or antiferromagnetic inter-dinuclear interactions [29,51–55].

The magnetic susceptibility data have been analyzed by means of the Hamiltonian given in Eq. (3) where J corresponds to the magnetic coupling constant between the two Mn(III) ions, D and g the uniaxial anisotropy and the Landé factor of a single Mn(III) ion respectively, and $S_1 = S_2 = S_{\text{Mn}}$ with S_{iz} for the z component of the S_i operator [29,55]

$$\hat{H} = -2JS_1S_2 + D_{\text{Mn}} \sum_{i=1,2} S_{iz}^2 + g\beta H \sum_{i=1,2} S_i \quad (3)$$

The dc magnetic susceptibility data were fitted using the MAGPACK code [56,57]. Intermolecular interactions were not considered due to the lack of an evident intermolecular exchange-path-way and in order to avoid overparameterization in the calculations. The best sets of parameters obtained are listed in Table 3.

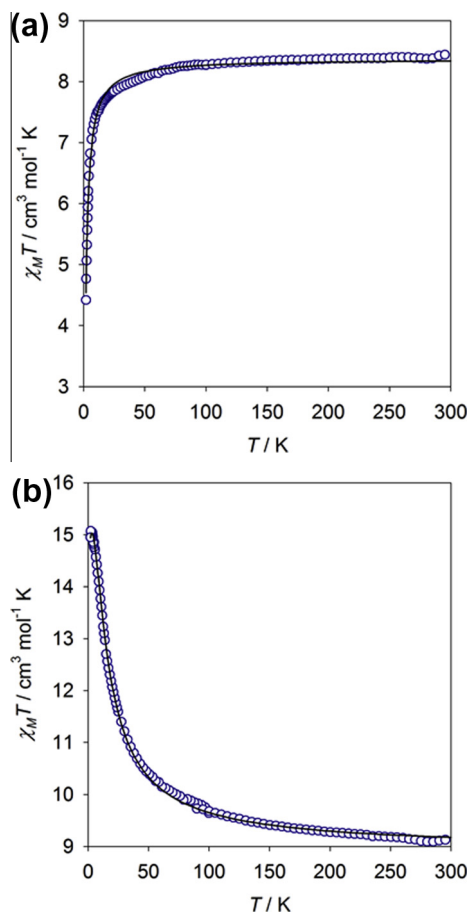


Fig. 7. Temperature dependence of the $\chi_M T$ product (per dinuclear unit) for compounds (a) **1** and (b) **2**. The solid line corresponds to the best fit to Eq. (1), see text.

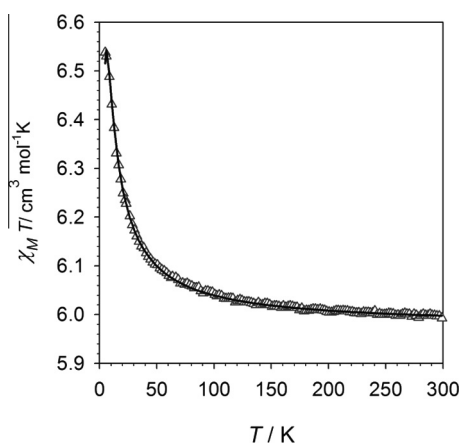


Fig. 8. Temperature dependence of the $\chi_M T$ product (per dinuclear unit) for compound **3** (the solid corresponds to the best fit to Eq. (3)). The inset shows the field dependence of magnetization of compound **3**.

Compounds **3** and **4** display weak ferromagnetic couplings between the Mn(III) ions with values in the range of other ferromagnetically coupled azido-bridged Mn(III) dinuclear compounds [29]. The values obtained for the $|D|$ parameter are consistent with the typical values which range from 0.2 to 2.53 cm^{-1} for those Mn(III) dinuclear complexes analogues [54,55]. We can observe that the calculated curves match very well the experimental data in the whole temperature range as can be seen in Figs. 8 and 9.

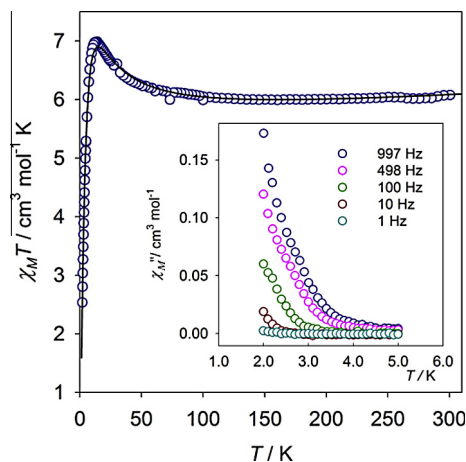


Fig. 9. Temperature dependence of the $\chi_M T$ product (per dinuclear unit) for compound **4**. The solid line corresponds to the best fit to the model (4), see text. The inset shows the out of phase magnetic susceptibilities vs. temperature plots for compound **4** under a *dc* field of 0 Oe and an *ac* field of 3.5 Oe.

Some ferromagnetically coupled Mn(III) dinuclear complexes have been observed to exhibit single molecule magnet (SMM) behavior [29,55]. In order to explore this possibility, *ac* magnetic susceptibility measurements were performed for compounds **3** and **4**. Compound **3** did not exhibit any out-of-phase *ac* signals, on the other hand, compound **4** exhibited frequency dependent *ac* signals which shifted the χ_M'' values to higher for higher frequencies, inset Fig. 9. However, a maximum for χ_M'' was not observed (in the temperature range and frequencies studied), which suggests the blocking temperature to fall below 2.0 K.

A qualitative explanation for the ferromagnetic coupling observed in **3** and **4** could be as follows. The Mn(III) ion in elongated octahedral geometry displays a $t_{2g}^3 e_g^1$ electronic configuration with a 5B_1 ground state due to the Jahn–Teller distortion. In these compounds the bridging azido groups connect an equatorial position of a Mn(III) ion (short distance) with an axial position of its nearest neighbor (long distance). In this sense, the azido bridge is coupling a d_π orbital ($d_{xy}d_{xz}d_{yz}$) with a d_z^2 orbital, which are orthogonal. This coupling usually yields weak ferromagnetic interactions due to the so-called strict orthogonality [2,29,54,58]. Quantitatively, the coupling is somewhat stronger in **4** since it exhibits shorter Mn–N_{azido} and shorter Mn···Mn intramolecular distances.

The temperature evolution of the $\chi_M T$ product for the compound **5** is shown in Fig. 10. At room temperature, $\chi_M T = 8.72(2) \text{ cm}^3 \text{ mol}^{-1} \text{ K}$ which corresponds well with spin-only value of $\chi_M T$ for Mn(II) ions with half-filled *d*-shell and $S = 5/2$ ($8.76 \text{ cm}^3 \text{ mol}^{-1} \text{ K}$). At low temperatures, a sharp maximum in the $\chi_M T$ curve is observed (at ~ 3 K), indicating the prevalence of antiferromagnetic exchange interactions. Thus, similarly to all other compounds studied, the magnetic behavior of the compound **5** is governed by competing ferromagnetic and antiferromagnetic interactions the strength of which significantly changes with the temperature. Like for compounds **1** and **2**, the profile of the $\chi_M T$ curve was analyzed by employing Eq. (1). The best fit parameters to Eq. (1) are $g = 2.02(1)$, $J = 0.87(2) \text{ cm}^{-1}$, $\theta = -0.61(1) \text{ K}$, and $R = 1.82 \times 10^{-5}$. The positive value of J implies ferromagnetic inter-

Table 3
Magnetic parameters for compounds **3** and **4**.

Compound	g	J (cm^{-1})	$ D $ (cm^{-1})	R
3	2.00	0.24	0.38	3.20×10^{-7}
4	1.95	3.23	0.50	3.05×10^{-5}

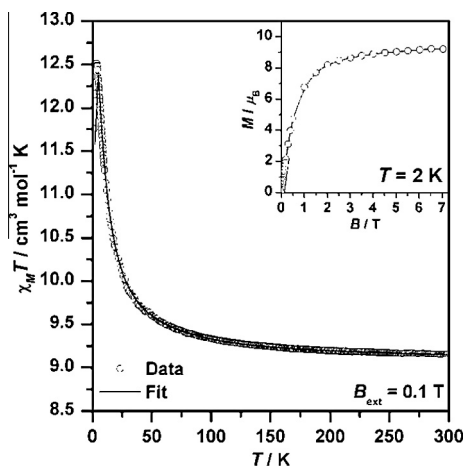


Fig. 10. Temperature dependence of the $\chi_M T$ product (per dinuclear unit) for compound **5** (the solid corresponds to the best fit to Eq. (1)). The inset shows the field dependence of magnetization of compound **5**.

actions favoring parallel arrangement of the binuclear unit. However, at low temperatures (below 3 K), antiferromagnetic interactions become strong enough to contribute to the magnetic response of the compound **5**. In increasing applied magnetic fields, the magnetization of the compound **5** approaches a value of $10 \mu_B$, expected for parallel arrangement within the binuclear unit.

4. Conclusions

When the four aroylhydrazone Schiff bases were employed in polynuclear synthesis with azide and Mn(II) (molar ratio 2:3) ions, the azide bridging ligand gave dinuclear Mn(II) and Mn(III) complexes, whereas using a low ratio of $N_3^-/Mn(II)$ gave a 2D coordination polymer without the azide bridge. Doubly bridged EO azides transmit ferromagnetic and antiferromagnetic couplings. In this work, a new two-dimensional manganese(II) coordination polymer has been synthesized with doubly deprotonated (*E*)-*N'*-(5-bromo-2-hydroxybenzylidene)isonicotinohydrazide, and the Mn(II) ion assumes a distorted octahedral coordination geometry. The two dimensional sheets pile up along [101] direction by the connection of adjacent sheets and form a super-molecular three-dimensional structure. The hydrogen bond between sheets consolidates the crystal.

Acknowledgments

The authors are grateful to the University of Zanjan, Universidad de La Laguna, Palacky University in Olomouc, the Faculty of Chemistry and Biochemistry of the Ludwig-Maximilians-Universität München and the School of Chemistry for financial support of this study. The authors gratefully acknowledge the support by the Operational Program Research and Development for Innovations – European Development Fund (Project No. CZ.1.05/2.1.00/03.0058) of the Ministry of Education, Youth, and Sports of the Czech Republic. We gratefully acknowledge the support by the Operational Program Research and Development for Innovations-European Regional Development Fund (project CZ.1.05/2.1.00/03.0058) and Operational Program Education for Competitiveness (CZ.1.07/2.3.00/20.0017).

Appendix A. Supplementary data

CCDC 899445, 899446, 899447, 899926, 899927 and 899448 contains the supplementary crystallographic data for this paper.

These data can be obtained free of charge via <http://www.ccdc.cam.ac.uk/conts/retrieving.html>, or from the Cambridge Crystallographic Data Centre, 12 Union Road, Cambridge CB2 1EZ, UK; fax: +44 1223 336 033; or e-mail: deposit@ccdc.cam.ac.uk. Supplementary data associated with this article can be found, in the online version, at <http://dx.doi.org/10.1016/j.poly.2013.05.033>.

References

- [1] M. Viciano Chumillas, S. Tanase, I. Mutikainen, U. Turpeinen, L.J. Jongh, J. Reedijk, *Inorg. Chem.* 47 (2008) 5919.
- [2] O. Kahn, *Molecular Magnetism*, Wiley-VCH, 1993.
- [3] H. Nagao, M. Nishino, Y. Shigeta, T. Soda, Y. Kitagawa, T. Onishi, Y. Yoshioka, K. Yamaguchi, *Coord. Chem. Rev.* 198 (2000) 265.
- [4] G. Aromi, M.J. Knapp, J.P. Claude, J.C. Huffman, D.N. Hendrickson, G. Christou, *J. Am. Chem. Soc.* 121 (1999) 5489.
- [5] A.J. Tasiopoulos, A. Vinslava, W. Wernsdorfer, K.A. Abboud, G. Christou, *Angew. Chem., Int. Ed.* 43 (2004) 2117.
- [6] P. Kar, P.M. Guha, M.G.B. Drew, T. Ishida, A. Ghosh, *Eur. J. Inorg. Chem.* (2011) 2075.
- [7] C. Beghidja, G. Rogez, J. Kortus, M. Wesolek, R. Welter, *J. Am. Chem. Soc.* 128 (2006) 3140.
- [8] M.N. Leuenberger, D. Loss, *Nature* 410 (2001) 789.
- [9] R. Biswas, S. Mukherjee, P. Kar, A. Ghosh, *Inorg. Chem.* 51 (2012) 8150.
- [10] A. Escuer, G. Aromi, *Eur. J. Inorg. Chem.* (2006) 4721.
- [11] S.-Q. Bai, C.-J. Fang, Z. He, E.-Q. Gao, C.-H. Yan, T.S.A. Hor, *Dalton Trans.* 41 (2012) 13379.
- [12] Z.-X. Li, Y.-F. Zeng, H. Ma, X.-H. Bu, *Chem. Commun.* 46 (2010) 8540.
- [13] S.-Q. Bai, C.-J. Fang, Z. He, E.-Q. Gao, C.-H. Yan, T.S.A. Hor, *CrystEngComm* 15 (2013) 650.
- [14] F. Meyer, S. Demeshko, G. Leibel, B. Kersting, E. Kaifer, H. Pritzko, *Chem. Eur. J.* 11 (2005) 1518.
- [15] P.K. Nanda, G. Aromi, D. Ray, *Chem. Commun.* (2006) 3181.
- [16] C. Adhikary, S. Koner, *Coord. Chem. Rev.* 254 (2010) 2933.
- [17] M. Mohan, M.P. Gupta, L. Chandra, N.K. Jha, *Inorg. Chim. Acta* 151 (1988) 61.
- [18] D.R. Richardson, P. Ponka, *Am. J. Hematol.* 58 (1988) 299.
- [19] D.S. Kalinowski, P.C. Sharpe, P.V. Bernhardt, D.R. Richardson, *J. Med. Chem.* 51 (2008) 331.
- [20] G. Tamasi, L. Chiasserini, L. Savini, A. Segal, R. Cini, *J. Inorg. Biochem.* 99 (2005) 1347.
- [21] M. Bakir, I. Hassan, T. Johnson, O. Brown, O. Green, C. Gyles, M.D. Coley, *J. Mol. Struct.* 688 (2004) 213.
- [22] O. Pouralimardan, A.-C. Chamayou, C. Janiak, H. Hosseini-Monfared, *Inorg. Chim. Acta* 360 (2007) 1599.
- [23] M.D. Ward, *J. Solid State Electrochem.* 9 (2005) 778.
- [24] P. Krishnamoorthy, P. Sathyadevi, R.R. Butorac, A.H. Cowley, N.S.P. Bhuvanesh, N. Dharmaraj, *Dalton Trans.* 41 (2012) 6842.
- [25] M.B. Hursthouse, S.A.A. Jayaweera, A. Quick, *Dalton Trans.* (1979) 279.
- [26] H. Hosseini-Monfared, S. Alavi, A. Farrokhi, M. Vahedpour, P. Mayer, *Polyhedron* 30 (2011) 1842.
- [27] S. Lin, S.-X. Liu, J.-Q. Huang, C.-C. Lin, *Dalton Trans.* (2002) 1595.
- [28] R. Bikas, H. Hosseini-Monfared, T. Lis, M. Siczek, *Inorg. Chem. Commun.* 15 (2012) 151.
- [29] C.-H. Ge, A.-L. Cui, Z.-H. Ni, Y.-B. Jiang, L.-F. Zhang, J. Ribas, H.-Z. Kou, *Inorg. Chem.* 45 (2006) 4883.
- [30] A. Ray, C. Rizzoli, G. Pilet, C. Desplanches, E. Garrriba, E. Rentschler, S. Mitra, *Eur. J. Inorg. Chem.* (2009) 2915.
- [31] L.N. Dawe, T.S.M. Abedin, T.L. Kelly, L.K. Thompson, D.O. Miller, L. Zhao, C. Wilson, M.A. Leech, J.A.K. Howard, *J. Mater. Chem.* 16 (2006) 2645.
- [32] G.M. Sheldrick, *Acta Crystallogr., Sect. A* 64 (2008) 112.
- [33] A. Altomare, M.C. Burla, M. Camalli, G.L. Casciarano, C. Giacovazzo, A. Guagliardi, A.G.G. Moliterni, G. Polidori, *Appl. Crystallogr.* 32 (1999) 115.
- [34] K. Brandenburg, *Diamond (Version 3.2d)*, Crystal, Molecular Structure Visualization, Crystal Impact – K. Brandenburg & H. Putz Gbr, Bonn (Germany), 2009.
- [35] S. Biswas, A.K. Dutta, K. Mitra, M.-C. Dul, S. Dutta, C.R. Lucas, B. Adhikary, *Inorg. Chim. Acta* 377 (2011) 56.
- [36] C.-M. Liu, D.-Q. Zhang, D.-B. Zhu, *Dalton Trans.* 39 (2010) 1781.
- [37] R. Bikas, H. Hosseini-Monfared, T. Lis, M. Siczek, *Acta Crystallogr., Sect. E: Struct. Rep. Online* 68 (2012) o367.
- [38] M. Habib, T.K. Karmakar, G. Aromi, J. Ribas-Arino, H.-K. Fun, S. Chantrapromma, S.K. Chandra, *Inorg. Chem.* 47 (2008) 4109.
- [39] Y. Song, C. Massera, O. Roubeau, P. Gamez, A.M.M. Lanfredi, J. Reedijk, *Inorg. Chem.* 43 (2004) 6842.
- [40] R.M. Silverstein, F.X. Webster, *Spectroscopic Identification of Organic Compounds*, sixth ed., Wiley, New York, 1998, p. 101.
- [41] H. Adams, D.E. Fenton, G. Minardi, E. Mura, A.M. Pistuddi, C. Solinas, *Inorg. Chem. Commun.* 3 (2000) 24.
- [42] G.C. Percy, D.A. Thornton, *J. Inorg. Nucl. Chem.* 34 (1972) 3369.
- [43] G. Kolawole, K.S. Patel, *Dalton Trans.* (1981) 1241.
- [44] S. Banerjee, A. Ray, S. Sen, S. Mitra, D.L. Hughes, R.J. Butcher, S.R. Batten, D.R. Turner, *Inorg. Chim. Acta* 361 (2008) 2692.

- [45] (a) Z.-S. Meng, L. Yun, W.-X. Zhang, C.-G. Hong, R. Herchel, Y.-C. Ou, J.-D. Leng, M.-X. Peng, Z.-J. Lin, M.-L. Tong, Dalton Trans. (2009) 10284;
(b) M.-M. Yu, Z.-H. Ni, C.-C. Zhao, A.-L. Cui, H.-Z. Kou, Eur. J. Inorg. Chem. (2007) 5670;
(c) T.K. Karmakar, B.K. Ghosh, A. Usman, H.-K. Fun, E. Riviere, T. Mallah, G. Aromi, S.K. Chandra, Inorg. Chem. 44 (2005) 2391.
- [46] S. Ray, S. Konar, A. Jana, S. Jana, A. Patra, S. Chatterjee, J.A. Golen, A.L. Rheingold, S.S. Mandal, S.K. Kar, Polyhedron 33 (2012) 82.
- [47] W.-J. Kang, J.-M. Dou, D.-C. Li, D.-Q. Wang, Acta Crystallogr., Sect. E: Struct. Rep. Online 63 (2007) o3328.
- [48] H. Hosseini-Monfared, R. Bikas, P. Mayer, Acta Crystallogr., Sect. E: Struct. Rep. Online 66 (2010) o236.
- [49] H. Hosseini-Monfared, S. Alavi, R. Bikas, M. Vahedpour, P. Mayer, Polyhedron 29 (2010) 3355.
- [50] E. Ruiz, J. Cano, S. Alvarez, P. Alemany, J. Am. Chem. Soc. 120 (1998) 5238.
- [51] R. Boca, Theoretical Foundations of Molecular Magnetism, Elsevier Science SA, Lausanne, Switzerland, 1999.
- [52] Y. Feng, C. Wang, Y. Zhao, J. Li, D. Liao, S. Yan, Q. Wang, Inorg. Chim. Acta 362 (2009) 3563.
- [53] G. Bhargavi, M.V. Rajasekharan, J.-P. Costes, J.-P. Tuchagues, Polyhedron 28 (2009) 1253.
- [54] S. Mandal, A. Rout, K.M. Fleck, G. Pilet, J. Ribas, D. Bandyopadhyay, Inorg. Chim. Acta 363 (2010) 2250.
- [55] Z. Lü, M. Yuan, F. Pan, S. Gao, D. Zhang, D. Zhu, Inorg. Chem. 45 (2006) 3538.
- [56] J.J. Borrás-Almenar, J.M. Clemente-Juan, E. Coronado, B.S. Tsukerblat, Inorg. Chem. 38 (1999) 6081.
- [57] J.J. Borrás-Almenar, J.M. Clemente-Juan, E. Coronado, B.S. Tsukerblat, J. Comput. Chem. 22 (2001) 985.
- [58] S. Saha, D. Mal, S. Koner, A. Bhattacharjee, P. Gutlich, S. Mondal, M. Mukherjee, K.I. Okamoto, Polyhedron 32 (2004) 1811.